

1 **Persistence of SARS CoV-2 S1 Protein in CD16+ Monocytes in Post-**  
2 **Acute Sequelae of COVID-19 (PASC) Up to 15 Months Post-Infection**

3

4 Bruce K. Patterson<sup>1</sup>, Edgar B. Francisco<sup>1</sup>, Ram Yogendra<sup>2</sup>, Emily Long<sup>1</sup>, Amruta Pise<sup>1</sup>, Hallison  
5 Rodrigues<sup>1</sup>, Eric Hall<sup>3</sup>, Monica Herrera<sup>3</sup>, Purvi Parikh<sup>4</sup>, , Jose Guevara-Coto<sup>5,6</sup>, Xaiolan Chang<sup>7</sup>,  
6 Jonah B Sacha<sup>7</sup>, Rodrigo A Mora-Rodríguez<sup>5</sup>, Javier Mora<sup>5</sup>

7

8

9 <sup>1</sup>IncellDx Inc, San Carlos, CA

10 <sup>2</sup>Lawrence General Hospital, Lawrence, MA

11 <sup>3</sup>Bio-Rad Laboratories, Hercules, CA

12 <sup>4</sup>NYU Langone Health, New York, NY

13 <sup>5</sup>Lab of Tumor Chemosensitivity, CIET / DC Lab, Faculty of Microbiology, Universidad de  
14 Costa Rica

15 <sup>6</sup>Department of Computer Science and Informatics (ECCI), Universidad de Costa Rica, San Jose,  
16 Costa Rica

17 <sup>7</sup> Vaccine & Gene Therapy Institute and Oregon National Primate Research Center, Oregon  
18 Health & Science University, Portland, OR, USA

19

20

21 **Summary: SARS CoV-2 S1 Protein in CD16+ Monocytes In PASC**

22

23

24 **Corresponding author:**

25 Bruce K. Patterson MD

26 1541 Industrial Road

27 San Carlos, CA 94070

28 Tel: +1.650.777.7630

29 Fax: +1.650.587.1528

30 Email: [brucep@incelldx.com](mailto:brucep@incelldx.com)

31

32 **Key words:**

33

34 COVID-19, PASC, SARS CoV-2 S1 Protein, non-classical monocytes, CCR5, fractalkine

35

36

37

38

39

40

41

42

43

44  
45  
46  
47  
48  
49  
50  
51  
52  
53  
54  
55  
56  
57  
58  
59  
60  
61  
62  
63  
64  
65  
66  
67  
68  
69  
70  
71  
72  
73  
74  
75  
76  
77  
78  
79  
80  
81  
82  
83  
84  
85  
86  
87

## ABSTRACT

The recent COVID-19 pandemic is a treatment challenge in the acute infection stage but the recognition of chronic COVID-19 symptoms termed post-acute sequelae SARS-CoV-2 infection (PASC) may affect up to 30% of all infected individuals. The underlying mechanism and source of this distinct immunologic condition three months or more after initial infection remains elusive. Here, we investigated the presence of SARS-CoV-2 S1 protein in 46 individuals. We analyzed T-cell, B-cell, and monocytic subsets in both severe COVID-19 patients and in patients with post-acute sequelae of COVID-19 (PASC). The levels of both intermediate (CD14+, CD16+) and non-classical monocyte (CD14Lo, CD16+) were significantly elevated in PASC patients up to 15 months post-acute infection compared to healthy controls ( $P=0.002$  and  $P=0.01$ , respectively). A statistically significant number of non-classical monocytes contained SARS-CoV-2 S1 protein in both severe ( $P=0.004$ ) and PASC patients ( $P=0.02$ ) out to 15 months post-infection. Non-classical monocytes were sorted from PASC patients using flow cytometric sorting and the SARS-CoV-2 S1 protein was confirmed by mass spectrometry. Cells from 4 out of 11 severe COVID-19 patients and 1 out of 26 also contained SARS-CoV-2 RNA. Non-classical monocytes are capable of causing inflammation throughout the body in response to fractalkine/CX3CL1 and RANTES/CCR5.

88 **INTRODUCTION**

89  
90 Post-acute sequelae SARS-CoV-2 infection (PASC) is a disabling and sometimes debilitating  
91 condition that occurs in 10%-30% of individuals infected by SARS-CoV-2 and has recently been  
92 proposed to cause neurologic symptoms in 30% of those infected<sup>1</sup>. The number and extent of  
93 symptoms is extremely heterogeneous with some reports suggesting >200 different symptoms<sup>2</sup>.  
94 The underlying cause of PASC symptoms has remained a mystery though some data has pointed  
95 to tissue reservoirs of persistent SARS-CoV-2 as a potential mechanism<sup>3,4</sup>. We recently reported  
96 a machine learning approach that identified the unique immunologic signature of individuals  
97 with PASC<sup>5</sup>. In the same report, we also identified characteristic immune cell subset  
98 abnormalities that accompanied the unique cytokine/chemokine profile. The predominant  
99 immune cell abnormality was elevations in monocyte subsets. Monocyte subpopulations are  
100 divided into 3 phenotypic and functionally distinct types. Classical monocytes exhibit the  
101 CD14<sup>++</sup>, CD16<sup>-</sup> phenotype, intermediate monocytes exhibit a CD14<sup>+</sup>, CD16<sup>+</sup> phenotype, and  
102 the non-classical monocytes express CD14<sup>lo</sup>, CD16<sup>+</sup><sup>6,7</sup>. Further they express very different cell  
103 surface markers as previously described. In particular, classical monocytes express high levels of  
104 the ACE-2 receptor, the putative receptor for SARS-CoV-2<sup>8</sup>. Intermediate and non-classical  
105 monocytes express very little ACE-2 receptor. Similarly, classical monocytes express low levels  
106 of the chemokine receptors CX3R1 and CCR5. Intermediate monocytes express high levels of  
107 CCR5 while non-classical monocytes express high levels of CX3R1. Here, we report kinetic  
108 differences in the proportions of monocyte subsets in severe cases and PASC, as well as the  
109 presence of SARS-CoV-2 protein in CD14<sup>lo</sup>, CD16<sup>+</sup> monocytes in PASC patients up to 16  
110 months post-acute SARS-CoV-2 infection.

111

112 **RESULTS**

113 Similar to other inflammatory and infectious conditions such as sepsis, lupus erythematosus, and  
114 rheumatoid arthritis among others<sup>9</sup>, we detected statistically significant increases ( $P < 0.002$ ) of  
115 intermediate CD14+, CD16+ monocytes in individuals with PASC compared to healthy controls.  
116 In addition, CD14lo, CD16+ non-classical monocytes were also significantly elevated in PASC  
117 ( $P = 0.01$ ). Neither intermediate nor non-classical monocytes were elevated in severe COVID-19  
118 (Figure 1).

119  
120 Since the reports by our group and others found that monocyte subsets can be infected by HIV,  
121 HCV, Zika virus and Dengue fever virus<sup>10-12</sup>, we screened peripheral blood mononuclear cells  
122 (PBMCs) from PASC individuals, as well as acute severe COVID-19 as controls, for SARS-  
123 CoV-2 RNA (Table 1). Using the highly sensitive, quantitative digital droplet PCR (ddPCR), we  
124 found that 36% (4 of 11) of severe COVID-19 patients' PBMCs contained SARS-CoV-2 RNA  
125 compared to 4% (1/26) of PASC patients' PBMCs. The one PASC patient that was RNA positive  
126 was 15 months post infection.

127  
128 To further establish the exact reservoir contributing to the positive signal detected using ddPCR,  
129 we performed high parameter flow cytometry with antibodies that define B cell, T-cell, and  
130 monocytic subsets in addition to simultaneous staining of these cells with an antibody for the  
131 SARS-CoV-2 S1 protein. As demonstrated in Figure 2, we found distinct subpopulations of  
132 SARS-CoV-2 containing cells in the CD14lo, CD16+ monocytic subset for 73% (19 out of 26)  
133 of PASC patients and 91% (10 out of 11) of severe COVID-19 patients. As demonstrated in  
134 Figure 3, the quantity of SARS-CoV-2 S1 containing cells were statistically significant in both

135 the severe patients (P=0.004) and in the PASC patients (P=0.02). Neither classical monocytes  
136 nor intermediate monocytes expressed the SARS-CoV-2 S1 protein.

137

138 To confirm the presence of SARS-CoV-2 S1 protein, we sorted CD14<sup>lo</sup>, CD16<sup>+</sup> monocytes and  
139 performed Ultra High-Performance Liquid Chromatography (UHPLC). Following  
140 immunoprecipitation, the elution fractions were dried down *in vacuo*, resuspended in ddH<sub>2</sub>O and  
141 purified by to remove any non-crosslinked SARS-CoV-2 S1 antibody as well as any detergents  
142 from the commercial immunoprecipitation buffers. The UHPLC collected fractions were dried *in*  
143 *vacuo*, resuspended in 100 mM HEPES (pH 8.0, 20% Acetonitrile), and subjected to cistern:  
144 reduction and alkylation with chloroacetamide. The samples were then digested with AspN and  
145 LysC endopeptidases for 16h at 37°C. The digested peptides were analyzed on an Agilent 6550  
146 IonFunnel QTOF and 1290 UHPLC by comparing patient samples to identical digests performed  
147 on commercially available SARS-CoV-2 S1 subunit. S1 subunit peptides from patient samples  
148 were mapped to a peptide database generated using commercial S1 subunit digests. Peptide  
149 identification consisted of matches in exact mass, isotope distribution, peptide charge state, and  
150 UHPLC retention time. As shown in Figure 4, the retention time of the representative peptide  
151 NLREFVFK in the digested commercial S1 subunit and Sample LH1-6 matched. Additionally,  
152 the Mass Spectra in Figure 4 show identical mass, isotope distribution, and charge states for the  
153 representative peptide NLREFVFK in the representative LH1 sample and commercial S1 subunit  
154 (also observed in LH 2-6, not shown). Using these metrics, up to 44% of the S1 subunit peptides  
155 could be identified in patient samples LH1-LH6 (Supplementary Table 1), providing  
156 complementary evidence to flow cytometry experiments that demonstrate the presence of S1  
157 subunit protein in these patient cells.

158

## 159 **DISCUSSION**

160 Here, we report the discovery of persistent SARS-CoV-2 protein in CD14<sup>lo</sup>, CD16<sup>+</sup> monocytes  
161 out to 15 months in some individuals and discuss the implications for the pathogenesis of PASC  
162 and severe cases of COVID-19. The three subtypes of circulating monocytes (classical,  
163 intermediate, non-classical) express very different cell surface molecules and serve very different  
164 functions in the immune system. Generally, classical' monocytes exhibit phagocytic activity,  
165 produce higher levels of ROS and secrete proinflammatory molecules such as IL-6, IL-8, CCL2,  
166 CCL3 and CCL5. Intermediate monocytes express the highest levels of CCR5 and are  
167 characterized by their antigen presentation capabilities, as well as the secretion of TNF- $\alpha$ , IL-1 $\beta$ ,  
168 IL-6, and CCL3 upon TLR stimulations. Non-classical monocytes expressing high levels of  
169 CX3CR1 are involved in complement and Fc gamma-mediated phagocytosis and anti-viral  
170 responses<sup>6</sup>.

171 After maturation, human monocytes are released from bone marrow into the circulation as  
172 classical monocytes. Currently, strong evidence supports the concept that intermediate and non-  
173 classical monocytes emerge sequentially from the pool of classical monocytes<sup>13</sup>. This is  
174 supported by transcriptome analysis showing that CD16<sup>+</sup> monocytes have a more mature  
175 phenotype<sup>14</sup>. In humans, 85% of the circulating monocyte pool are classical monocytes, whereas  
176 the remaining 15% consist of intermediate and nonclassical monocytes<sup>13</sup>. Classical monocytes  
177 have a circulating lifespan of approximately one day before they either migrate into tissues, die,  
178 or turn into intermediate and subsequently nonclassical monocytes<sup>6,13</sup>.

179 During pathologic conditions mediated by infectious/inflammatory reactions, the proportions of  
180 monocyte subsets vary according to the functionality of each specific subpopulation<sup>6,13,15</sup>. Our

181 previous results show that during early stages of the disease, PASC group have reduced classical  
182 monocyte and increased intermediate monocyte percentages compared with healthy controls<sup>5</sup>.  
183 Here, we report an increase in nonclassical monocytes in PASC group 6-15 months post  
184 infection, and higher percentages of intermediate and nonclassical monocytes at day 0 in severe  
185 cases, suggesting augmented classical-intermediate-nonclassical monocyte transition in both  
186 groups but with different kinetics.

187 The clinical relevance of monocyte activation in COVID-19 patients and the significance of  
188 these cells as viral protein reservoir in PASC is supported by our data reporting the presence of  
189 S1 protein within nonclassical monocytes. Viral particles and/or viral proteins can enter  
190 monocyte subpopulations in distinct ways, and this appears to be regulated differently in  
191 individuals that will develop severe disease or PASC. Classical monocytes are primarily  
192 phagocytes and express high levels of the ACE-2 receptor<sup>8</sup>. Therefore, they could either  
193 phagocyte viral particles and apoptotic virally infected cells or be potential targets for SARS-  
194 CoV-2 infection. Considering their short circulating lifespan, viral protein-containing classic  
195 monocytes turn into intermediate and nonclassical monocytes. According to our results, this  
196 process happens faster in the severe group than in the PASC group. Indeed, at early stages of the  
197 disease the severe group show increased nonclassical monocytes whereas in PASC both the  
198 intermediate monocytes and non-classical monocytes are elevated. Additionally, CD14+CD16+  
199 monocytes express intermediate levels of ACE-2 receptors and could as well serve as an  
200 infectious target of SARS-CoV-2 as it has been proved to be an infectious target of HIV-1 and  
201 HCV<sup>11</sup>. Nonclassical monocytes have been proposed to act as custodians of vasculature by  
202 patrolling endothelial cell integrity<sup>16</sup>, thus pre-existing CD14<sup>lo</sup> CD16<sup>+</sup> cells could ingest virally  
203 infected apoptotic endothelial cells augmenting the proportion of nonclassical monocytes

204 containing S1 protein. This mechanism is more likely to take place in the PASC group where the  
205 S1 protein was detected 12-15 months post infection than in the severe group. Furthermore,  
206 nonclassical monocytes are associated with FcR-mediated phagocytosis<sup>17,18</sup>, which might be  
207 related with the ingestion of opsonized viral particles after antibody production at later stages of  
208 the disease in PASC.

209 Previous reports indicate that the numbers of classical monocytes decrease, but the numbers of  
210 intermediate and non-classical monocytes increase in COVID-19 patients<sup>19</sup>. Thus, the presence  
211 of S1 protein in nonclassical monocytes in both severe and PASC, might be associated with  
212 clinical characteristics and outcome of these groups. Previously, we found that individuals with  
213 severe COVID-19 have high systemic levels of IL-6, IL-10, VEGF and sCD40L<sup>5</sup>. Consistent  
214 with our data, other studies showed association of increased production of IL-6, VEGF and IL-10  
215 by nonclassical monocytes with disease severity<sup>20-22</sup>

216 In the case of PASC, the persistence of circulating S1-containing nonclassical monocytes up to  
217 16 months post infection, independently of the different possible mechanisms of viral proteins  
218 internalization discussed above, indicates that certain conditions are required to maintain this cell  
219 population. It has been shown in both humans and mice that nonclassical monocytes require  
220 fractalkine (CX3CL1) and TNF to inhibit apoptosis and promote cell survival<sup>22</sup>. Our previous  
221 data show high IFN- $\gamma$  levels in PASC individuals<sup>5</sup>, which can induce TNF- $\alpha$  production<sup>23</sup>.

222 Further, TNF- $\alpha$  and IFN- $\gamma$  induce CX3CL1/Fractalkine production by vascular endothelial cells<sup>24</sup>  
223 creating the conditions to promote survival of nonclassical monocytes. Another important aspect  
224 is the permanency of S1-containing cells in the circulation, intermediate monocytes express high  
225 levels of CCR5 and extravasation of these cells can occur in response to CCL4 gradients. We  
226 showed that PASC individuals have low levels of CCL4<sup>5</sup> maintaining these cells in circulation



227 until they turn into nonclassical monocytes. Moreover, IFN- $\gamma$  induced CX3CL1/Fractalkine  
228 production by endothelial cells<sup>23</sup> creates a gradient within the vascular compartment preserving  
229 nonclassical monocytes expressing CX3CR1 in the circulation.

230 Nonclassical monocytes are usually referred as anti-inflammatory cells<sup>22</sup>, nevertheless it was  
231 recently shown that this subset can acquire a proinflammatory phenotype<sup>25</sup>. Nonclassical  
232 monocytes acquire hallmarks of cellular senescence, which promote long term survival of these  
233 cells in circulation as explained above. Additionally, this induces an inflammatory state of the  
234 non-classical monocytes that could be a manifestation of the senescence-associated secretory  
235 phenotype (SASP), characterized by a high basal NF- $\kappa$ B activity and production of pro-  
236 inflammatory cytokines such as IL-1 $\alpha$ , TNF- $\alpha$  and IL-8<sup>25</sup>.

237 The hallmark of PASC is the heterogeneity of symptoms arising in a variety of tissues and  
238 organs. These symptoms are likely associated with the inflammatory phenotype of these  
239 senescent nonclassical monocytes. The CD14lo, CD16+, S1 protein+ monocytes could be  
240 preferentially recruited into anatomic sites expressing fractalkine and contribute to vascular and  
241 tissue injury during pathological conditions in which this monocyte subset is expanded as  
242 previously demonstrated in non-classical monocytes without S1 protein. Previously, CD16+  
243 monocytes were demonstrated to migrate into the brain of AIDS patients expressing high levels  
244 of CX3CL1 (fractalkine) and SDF-1<sup>26</sup>, and mediate blood-brain barrier damage and neuronal  
245 injury in HIV-associated dementia via their release of proinflammatory cytokines and neurotoxic  
246 factors. These sequelae are very common in PASC and these data could represent the underlying  
247 mechanism for the symptoms. Interestingly, a number of papers have been written discussing the  
248 increased mobilization of CD14lo, CD16+ monocytes with exercise<sup>27</sup>. These data support the  
249 reports of worsening PASC symptoms in individuals resuming pre-COVID exercise regimens. In

250 summary, the mechanism of PASC discussed in this report suggests that intermediate monocytes  
251 remain in circulation due to low CCL4 levels extending their time to differentiate leading to an  
252 accumulation of non-classical monocytes. The utility of using CCR5 antagonists in preventing  
253 migration of intermediate and non-classical monocytes due to the elevated levels of  
254 CCL5/RANTES in PASC<sup>5</sup>. Further, our data suggests that interruption of the  
255 CX3CR1/fractalkine pathway would be a potential therapeutic target to reduce the survival of  
256 S1-containing non-classical monocytes and the associated vascular inflammation previously  
257 discussed<sup>5</sup> and presented here.

258

## 259 **MATERIAL/METHODS**

### 260 *Patients*

261 Following informed consent, whole blood was collected in a 10 mL EDTA tube and a 10 mL plasma  
262 preparation tube (PPT). A total of 144 individuals were enrolled in the study consisting of 29 normal  
263 individuals, 26 mild-moderate COVID-19 patients, 25 severe COVID-19 patients and 64 chronic COVID  
264 (long hauler-LH) individuals. Long Haulers symptoms are listed in Figure 1. Study subjects were  
265 stratified according to the following criteria.

### 266 Mild

- 267 1. Fever, cough, sore throat, malaise, headache, myalgia, nausea, diarrhea, loss of taste and smell
- 268 2. No sign of pneumonia on chest imaging (CXR or CT Chest)
- 269 3. No shortness of breath or dyspnea

### 270 Moderate:

- 271 1. Radiological findings of pneumonia fever and respiratory symptoms
- 272 2. Saturation of oxygen (SpO<sub>2</sub>) ≥ 94% on room air at sea level

### 273 Severe

- 274 1. Saturation of oxygen (SpO<sub>2</sub>) < 94% on room air at sea level
- 275 2. Arterial partial pressure of oxygen (PaO<sub>2</sub>)/ fraction of inspired oxygen (FiO<sub>2</sub>) < 300mmHG
- 276 3. Lung infiltrate > 50% within 24 to 48 hours
- 277 4. HR ≥ 125 bpm
- 278 5. Respiratory rate ≥ 30 breaths per minute

279 Critical

- 280 1. Respiratory failure and requiring mechanical ventilation, ECMO, high-flow nasal cannula oxygen
- 281 supplementation, noninvasive positive pressure ventilation (BiPAP, CPAP)
- 282 2. Septic Shock- Systolic blood pressure < 90mmHg or Diastolic blood pressure < 60 mmHg or
- 283 requiring vasopressors (levophed, vasopressin, epinephrine)
- 284 3. Multiple organ dysfunction (cardiac, hepatic, renal, CNS, thrombotic disease)

285

286 Post-acute COVID-19 (Long COVID)

- 287 1. Extending beyond 3 weeks from the initial onset of first symptoms

288 Chronic COVID-19

- 289 1. Extending beyond 12 weeks from the initial onset of first symptoms (Table 1S)

290

291 *High Parameter Immune Profiling/Flow Cytometry*

292 Peripheral blood mononuclear cells were isolated from peripheral blood using Lymphoprep density  
293 gradient (STEMCELL Technologies, Vancouver, Canada). Aliquots 200 of cells were frozen in media  
294 that contained 90% fetal bovine serum (HyClone, Logan, UT) and 10% dimethyl sulfoxide (Sigma-  
295 Aldrich, St. Louis, MO) and stored at -70°C. Cells were stained and analyzed using a 17-color antibody  
296 cocktail (Supplementary Table 1) including a PE-labeled SARS-CoV-2 S1 antibody (Supplementary  
297 Table 1).

298 *Digital Droplet PCR*

299 A QIAamp Viral Mini Kit (Qiagen, Catalog #52906) was used to extract nucleic acids from 300 to 400  
300 mL of plasma sample according to the manufacturer's instructions and eluted in 50 mL of AVE buffer  
301 (RNase-free water with 0.04% sodium azide). The purified nucleic acids were tested immediately with a  
302 Bio-Rad SARS-CoV-2 ddPCR Kit (Bio-Rad, Hercules, CA, USA). The panel was designed for  
303 specifically detecting 2019-nCoV (two primer/probe sets). An additional primer/probe set was used to  
304 detect the human RNase P gene in control samples and clinical specimens. RNA isolated and purified  
305 from the plasma samples (5.5 mL) was added to a master mix comprising 1.1 mL of 2019-nCoV triplex  
306 assay, 2.2 mL of reverse transcriptase, 5.5 mL of supermix, 1.1 mL of dithiothreitol, and 6.6 mL of  
307 nuclease-free water.

308 The mixtures were then fractionated into up to 20,000 nanoliter-sized droplets in the form of a water-in-  
309 oil emulsion in a QX200 Automated Droplet Generator (Bio-Rad, Hercules, CA). The 96-well real-time-  
310 digital droplet polymerase chain reaction (RT-ddPCR) ready plate containing droplets was sealed with  
311 foil using a plate sealer and thermocycled to reverse transcribe the RNA, before PCR amplification of  
312 cDNA in a C1000 Touch thermocycler (Bio-Rad, Hercules, CA, USA). After PCR, the plate was loaded  
313 into a QX200 Droplet Reader (Bio-Rad, Hercules, CA, USA) and the fluorescence intensity of each  
314 droplet was measured in two channels (FAM and HEX). The fluorescence data were then analyzed with  
315 QuantaSoft 1.7 and QuantaSoft Analysis Pro 1.0 Software (Bio-Rad, Hercules, CA, USA).

316

317 *Flow Cytometric Cell Sorting*

318 Cryopreserved PBMCs were quick-thawed, centrifuged, and washed in 2% BSA solution in D-  
319 PBS. Cells were blocked for 5 min. in 2% BSA and then incubated at room temperature for 30  
320 min. with Alexa Fluor® 488 Anti-CD45 antibody (IncellDx, 1/100 dilution), 2.5 ug of Alexa  
321 Fluor® 647 Anti-CD16 antibody (BD, Cat. # 55710), and 1 ug of PerCP/Cy5.5 Anti-human  
322 CD14 antibody (Biolegend, Cat. #325622). Cells were washed twice with 2% BSA/D-PBS,

323 filtered, and kept on ice for the duration of the cell sort. Data was acquired on a Sony SH800,  
324 and only CD45+ cells staining positive for both CD14+ and CD16+ were sorted into test tubes  
325 with 100 uL 2% BSA solution. Sort purity of control PBMCs was confirmed to be >99% by re-  
326 analyzing sorted PBMCs using the same template and gating strategy.

327

### 328 *Single Cell Protein Identification*

329

330 Patient cells were sorted based on phenotypic markers (as above) and frozen at -80° C. Six  
331 patient samples with positive flow cytometry signal and sufficient cell counts were chosen for  
332 LCMS confirmation. Frozen cells were lysed with the IP Lysis/Wash Buffer from the kit  
333 according to the manufacturer's protocol. 10 ug of anti-S1 mAb were used to immunoprecipitate  
334 the S1 Spike protein from cell lysate of each patient. After overnight incubation with end-over-  
335 end rotation at 4°C and then three washes with IP Lysis/Wash Buffer, bound S1 Spike protein  
336 was eluted with the elution buffer from the kit.

337 IP elution fractions were dried *in vacuo*, resuspended in 20 uL of water, pooled, and purified by  
338 Agilent 1290 UPLC Infinity II on a Discovery C8 (3cm x 2.1 mm, 5 µm, Sigma-Aldrich, room  
339 temperature) using mobile phase solvents of 0.1% trifluoroacetic acid (TFA) in water or  
340 acetonitrile. The gradient is as follows: 5-75% acetonitrile (0.1% TFA) in 4.5 min (0.8 mL/min),  
341 with an initial hold at 5% acetonitrile (0.1% TFA) for 0.5 min (0.8 mL/min). The purified protein  
342 was dried *in vacuo* and resuspended in 50 µL of 100 mM HEPES, pH 8.0 (20% Acetonitrile). 1  
343 µL of TCEP (100 mM) was added and the samples were incubated at 37°C for 30 min. 1 µL of  
344 chloroacetamide (500 mM) was added to the samples and incubated at room temperature for 30

345 min. 1  $\mu$ L rAspN (Promega 0.5  $\mu$ g/ $\mu$ L) and 1  $\mu$ L of LysC (Pierce, 1  $\mu$ g/ $\mu$ L) were added and the  
346 samples incubated at 37°C for 16 h, prior to LCMS analysis.

347

#### 348 *LC-MS analysis*

349 Digested recombinant SARS-CoV-2 Spike S1 protein was analyzed by a high mass accuracy  
350 mass spectrometer to generate a list of detectable peptides with retention time and accurate  
351 masses. An Agilent 1290 Infinity II high pressure liquid chromatography (HPLC) system and an  
352 AdvanceBio Peptide Mapping column (2.1  $\times$  150 mm, 2.7  $\mu$ m) were used for peptide separation  
353 prior to mass analysis. The mobile phase used for peptide separation consists of a solvent A  
354 (0.1% formic acid in H<sub>2</sub>O) and a solvent B (0.1% formic acid in 90% CH<sub>3</sub>CN). The gradient was  
355 as follows: 0–1 min, 3% B; 1– 30 min, to 40% B; 30–33 min, to 90% B; 33-35 min, 90% B; 37-  
356 39 min, 3% B. Eluted peptides were electrosprayed using a Dual JetStream ESI source coupled  
357 with the Agilent 6550 iFunnel time-of-flight MS analyzer. Data was acquired using the MS  
358 method in 2 GHz (extended dynamic range) mode over a mass/charge range of 50–1700 Daltons  
359 and an auto MS/MS method. Acquired data were saved in both centroid and profile mode using  
360 Agilent Masshunter Workstation B09 Data acquisition Software. The same analytical method  
361 was applied to immunoprecipitated samples from sorted patient cells except no ms/ms was  
362 acquired.

363

364

#### 365 **REFERENCES**

366

- 367 1. Rubin R. As Their Numbers Grow, COVID-19 “Long Haulers” Stump  
368 Experts. *JAMA*. 2020;**324**:1381–83. doi:10.1001/jama.2020.17709
- 369 2. <https://www.cdc.gov/coronavirus/2019-ncov/hcp/clinical-care/post-covid-conditions.html>  
370 (April 8, 2021).
- 371 3. Yao XH, He ZC, Li TY, et. al.. Pathological evidence for residual SARS-CoV-2 in  
372 pulmonary tissues of a ready-for-discharge patient. *Cell Res*. 2020;**30**:541-43. doi:  
373 10.1038/s41422-020-0318-5. Epub 2020 Apr 28. PMID: 32346074; PMCID:  
374 PMC7186763.
- 375 4. Nienhold R, Ciani Y, Koelzer VH, et. al. Two distinct immunopathological profiles in  
376 autopsy lungs of COVID-19. *Nat Commun*. 2020; 11:5086. doi: 10.1038/s41467-020-  
377 18854-2.
- 378 5. Patterson BK, Guevarra-Coto J, Yogendra R. et al. Immune-based prediction of COVID-  
379 19 severity and chronicity decoded using machine learning. *Front Immunol in press*
- 380 6. Kapellos TS, Bonaguro L, Gemünd I, et. al. Human monocyte subsets and phenotypes in  
381 major chronic inflammatory diseases. *Front Immunol* 2019;**10**:1–13.  
382 <https://doi.org/10.3389/fimmu.2019.02035>
- 383 7. Ziegler-Heitbrock L. The CD14+ CD16+ blood monocytes: their role in infection and  
384 inflammation. *Journal of Leukocyte Biology* 2007;**81**:584–92.  
385 <https://doi.org/10.1189/jlb.0806510>
- 386 8. Rutkowska-Zapala M, Suski M, Szatanek R, et. al. Human monocyte subsets exhibit  
387 divergent angiotensin I-converting activity *Clin Exp Immunol* 2015;**181**: 126–32.
- 388 9. Mukherjee R, Kanti Barman P, Kumar Thatoi P, et. al. Non-Classical monocytes display  
389 inflammatory features: Validation in Sepsis and Systemic Lupus Erythematosus. *Sci Rep*.  
390 2015;**5**:13886. doi: 10.1038/srep13886.
- 391 10. Michlmayr D, Andrade P, Gonzalez K, et. al. CD14+CD16+ monocytes are the main  
392 target of Zika virus infection in peripheral blood mononuclear cells in a paediatric study  
393 in Nicaragua. *Nature Microbiology*, 2017;**2**:1462–70. [https://doi.org/10.1038/s41564-](https://doi.org/10.1038/s41564-017-0035-0)  
394 [017-0035-0](https://doi.org/10.1038/s41564-017-0035-0)
- 395 11. Coquillard G, Patterson BK. Determination of hepatitis C virus-infected, monocyte  
396 lineage reservoirs in individuals with or without HIV coinfection. *J Infect Dis*. 2009;  
397 **200**:947-54. doi: 10.1086/605476. PMID: 19678757
- 398 12. Ancuta P, Kunstman KJ, Autissier P, et. al. CD16+ monocytes exposed to HIV promote  
399 highly efficient viral replication upon differentiation into macrophages and interaction  
400 with T cells. *Virology* 2006;**344**:267–76. <https://doi.org/10.1016/j.virol.2005.10.027>
- 401 13. Patel AA, Zhang Y, Fullerton JN, et. al. The fate and lifespan of human monocyte subsets  
402 in steady state and systemic inflammation. *J Exp Med*. 2017;**214**:1913-23. doi:  
403 10.1084/jem.20170355. Epub 2017 Jun 12. PMID: 28606987; PMCID: PMC5502436.
- 404 14. Ancuta P, Liu KY, Misra V, Wacleche VS, Gosselin A, Zhou X, Gabuzda D.  
405 Transcriptional profiling reveals developmental relationship and distinct biological  
406 functions of CD16+ and CD16- monocyte subsets. *BMC Genomics* 2009;**10**:403. doi:  
407 10.1186/1471-2164-10-403. PMID: 19712453; PMCID: PMC2741492.
- 408 15. Tak T, van Groenendael R, Pickkers P, et. al. Monocyte subsets are differentially lost  
409 from the circulation during acute inflammation induced by human experimental  
410 endotoxemia. *J Innate Immun*. 2017;**9**:464-74. doi: 10.1159/000475665. Epub 2017 Jun  
411 23. PMID: 28641299; PMCID: PMC6738874.



- 412 16. Auffray C, Fogg D, Garfa M, et. al. Monitoring of blood vessels and tissues by a  
413 population of monocytes with patrolling behavior. *Science* 2007;**317**:666-70. doi:  
414 10.1126/science.1142883. PMID: 17673663.
- 415 17. Gren ST, Rasmussen TB, Janciauskiene S, A single-cell gene-expression profile reveals  
416 inter-cellular heterogeneity within human monocyte subsets. *PLoS One*  
417 2015;**10**:e0144351. doi: 10.1371/journal.pone.0144351. PMID: 26650546; PMCID:  
418 PMC4674153.
- 419 18. Wong KL, Tai JJ, Wong WC, et. al.. Gene expression profiling reveals the defining  
420 features of the classical, intermediate, and nonclassical human monocyte subsets. *Blood*.  
421 2011;**118**:e16-31. doi: 10.1182/blood-2010-12-326355. Epub 2011 Jun 7. PMID:  
422 21653326.
- 423 19. Jafarzadeh A, Chauhan P, Saha B, et. al.. Contribution of monocytes and macrophages to  
424 the local tissue inflammation and cytokine storm in COVID-19: Lessons from SARS and  
425 MERS, and potential therapeutic interventions. *Life Sci*. 2020;**257**:118102. doi:  
426 10.1016/j.lfs.2020.118102. Epub 2020 Jul 18. PMID: 32687918; PMCID: PMC7367812.
- 427 20. Zhou Y, Fu B, Zheng X, et. al. Pathogenic T-cells and inflammatory monocytes incite  
428 inflammatory storms in severe COVID-19 patients, *National Science Review*  
429 2020;**7**:998–1002
- 430 21. Olingy CE, San Emeterio CL, Ogle ME, et. al. Non-classical monocytes are biased  
431 progenitors of wound healing macrophages during soft tissue injury. *Sci Rep*. 2017;**7**:447.  
432 doi: 10.1038/s41598-017-00477-1. PMID: 28348370; PMCID: PMC5428475.
- 433 22. Narasimhan PB, Marcovecchio P, Anouk AAJ, et. al. Nonclassical monocytes in health  
434 and disease. *Ann Rev Immunol* 2019;**37**:439-56.
- 435 23. Vila-del Sol V, Punzón C, Fresno M. IFN-gamma-induced TNF-alpha expression is  
436 regulated by interferon regulatory factors 1 and 8 in mouse macrophages. *J Immunol*  
437 2008;**181**:4461-70. doi: 10.4049/jimmunol.181.7.4461. PMID: 18802049.
- 438 24. Matsumiya T, Ota K, Imaizumi T, et. al. Characterization of Synergistic Induction of  
439 CX3CL1/Fractalkine by TNF- $\alpha$  and IFN- $\gamma$  in vascular endothelial cells: an essential role  
440 for TNF- $\alpha$  in post-transcriptional regulation of CX3CL1. *J Immunol* 2010;**184**:4205-  
441 14; DOI: 10.4049/jimmunol.0903212
- 442 25. Ong SM, Hadadi E, Dang TM, et. al.. The pro-inflammatory phenotype of the human  
443 non-classical monocyte subset is attributed to senescence. 2008 *Cell Death Dis* **9**:266  
444 <https://doi.org/10.1038/s41419-018-0327-1>
- 445 26. Pereira CF, Middel J, Jansen G, et. al. Enhanced expression of fractalkine in HIV-1  
446 associated dementia. *J Neuroimmunol* 2001;**115**:168-75. doi: 10.1016/s0165-  
447 5728(01)00262-4. PMID: 11282167.
- 448 27. Jajtner AR, Townsend JR, Beyer KS, et. al. Resistance exercise selectively mobilizes  
449 monocyte subsets: role of polyphenols. *Med Sci Sports Exerc*. 2018;**50**:2231-41. doi:  
450 10.1249/MSS.0000000000001703. PMID: 29957728.

451  
452 **Ethics**

453 Informed consent was obtained from all participants.

454

455 **Data and materials availability:**

456 All requests for materials and raw data should be addressed to the corresponding author



457  
458  
459  
460  
461  
462  
463  
464  
465  
466  
467  
468  
469  
470  
471  
472  
473  
474  
475  
476  
477  
478  
479  
480  
481  
482  
483  
484  
485  
486  
487  
488  
489  
490  
491  
492  
493  
494  
495  
496  
497  
498  
499  
500  
501  
502  
503

**Competing interests:**

B.K.P, A.P., H.R., E.L, and EBF. are employees of IncellDx

**Author contributions:**

R.Y. and P.P. organized the clinical study and actively recruited patients.

B.K.P, A.P., H.R., X.E, E.L., J.B.S. performed experiments and analyzed the data.

J.G-C., R.A.M., J.M. performed the statistics and bioinformatics

B.K.P., J.M., EBF, J.G-C., R.A.M. wrote the draft of the manuscript and all authors contributed to revising the manuscript prior to submission.

**Funding:** None

504  
505  
506  
507  
508  
509

**TABLE and FIGURE LEGENDS**

Table 1. Molecular analysis of study participants.

COVID-19 Status	Sars-CoV-2 RNA+		Months Post-Infection
	NS	PBMCs	
HC 1	-	-	n/a
HC 2	-	-	n/a
HC 3	-	-	n/a
HC 4	-	-	n/a
HC 5	-	-	n/a
HC 6	-	-	n/a
HC 7	-	-	n/a
HC 8	-	-	n/a
Asymptomatic	+	+	n/a
Severe 1	+	-	n/a
Severe 2	+	+	n/a
Severe 3	+	-	n/a
Severe 4	+	-	n/a
Severe 5	+	-	n/a
Severe 6	+	-	n/a
Severe 7	+	+	n/a
Severe 8	+	-	n/a
Severe 9	+	-	n/a
Severe 10	+	+	n/a
Severe 11	+	+	n/a
LH 1	+	-	13
LH 2	+	-	14
LH 3	+	-	6
LH 4	+	-	11
LH 5	+	+	15
LH 6	+	-	13
LH 7	+	-	12
LH 8	+	-	7
LH 9	+	-	14
LH 10	+	-	13
LH 11	+	-	12
LH 12	+	-	12
LH 13	+	-	6
LH 14	+	-	14
LH 15	+	-	13

LH 16	+	-	9
LH 17	+	-	11
LH 18	+	-	7
LH 19	+	-	14
LH 20	+	-	11
LH 21	+	-	13
LH 22	+	-	10
LH 23	+	-	8
LH 24	+	-	7
LH 25	+	-	12
LH 26	+	-	15

---

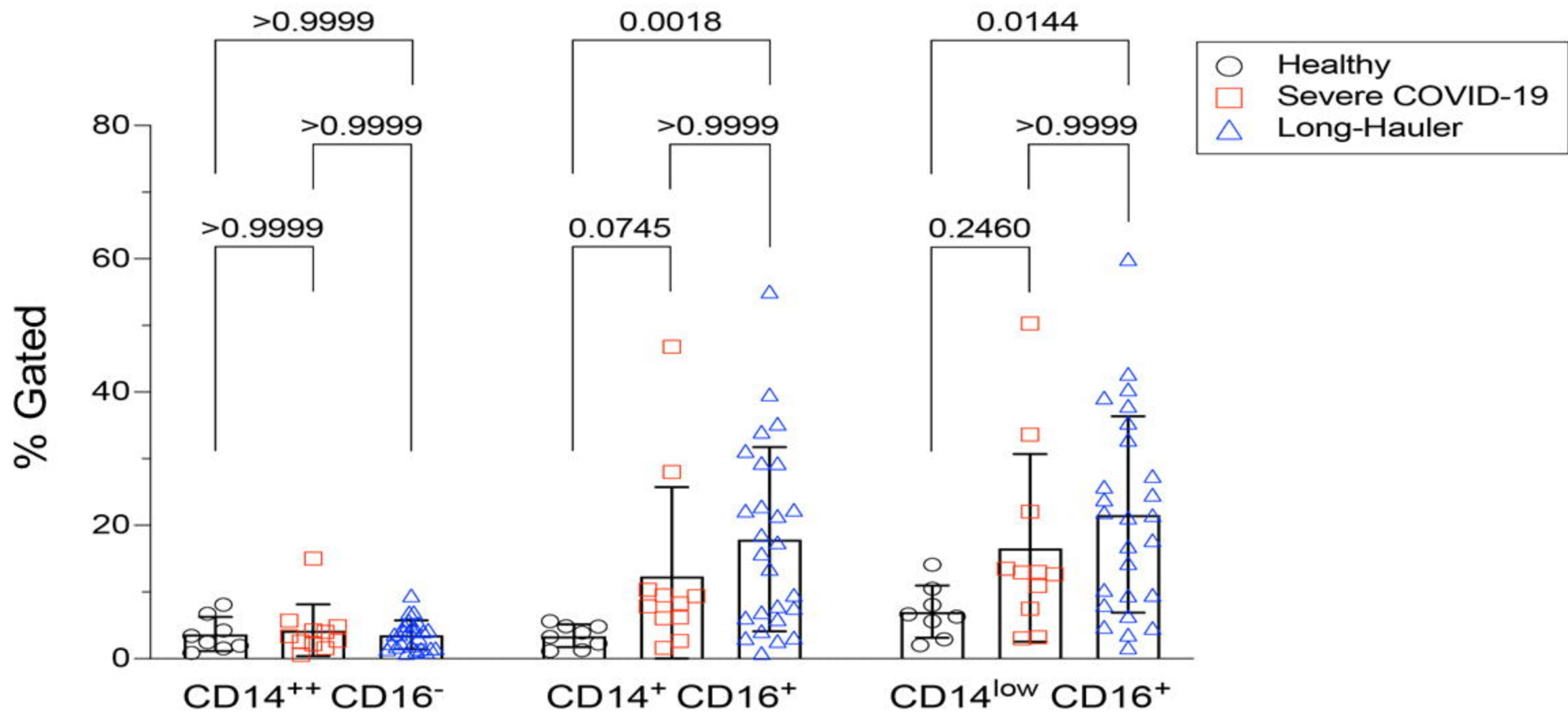
510 **Figure 1.** Quantification of classical, intermediate and non-classical monocytes in PASC (LH).  
511 Non-classical monocytes were significantly elevated in severe COVID-19 and in PASC.

512  
513 **Figure 2.** High parameter flow cytometric quantification of SARS-CoV-2 S1 protein in  
514 monocytic subsets. Cells were gated on CD45 then analyzed for CD14 and CD16 expression.  
515 Classical monocytes are green, intermediate monocytes are red and non-classical monocytes are  
516 blue.

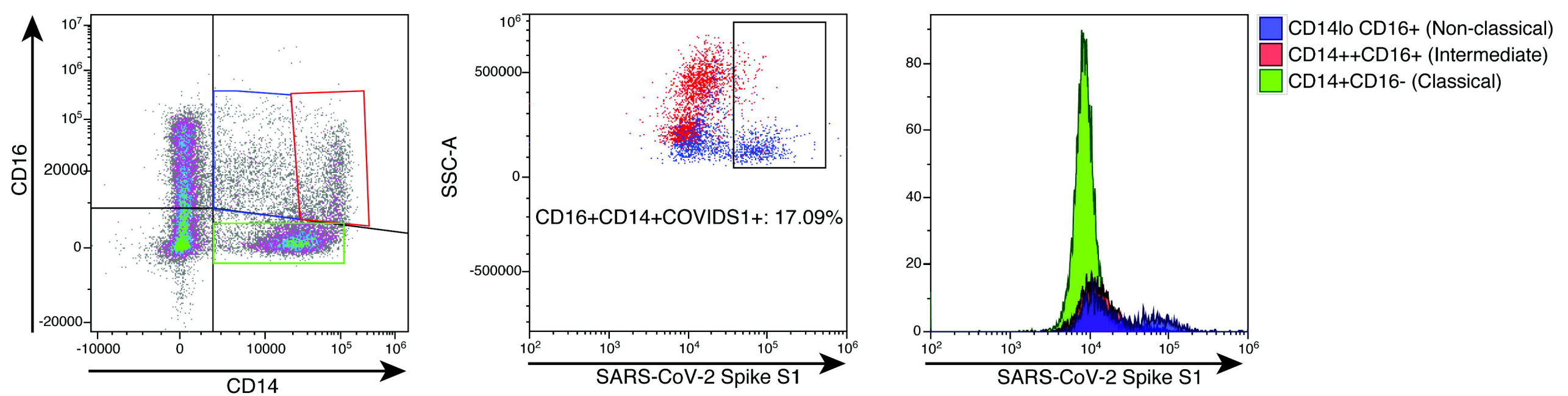
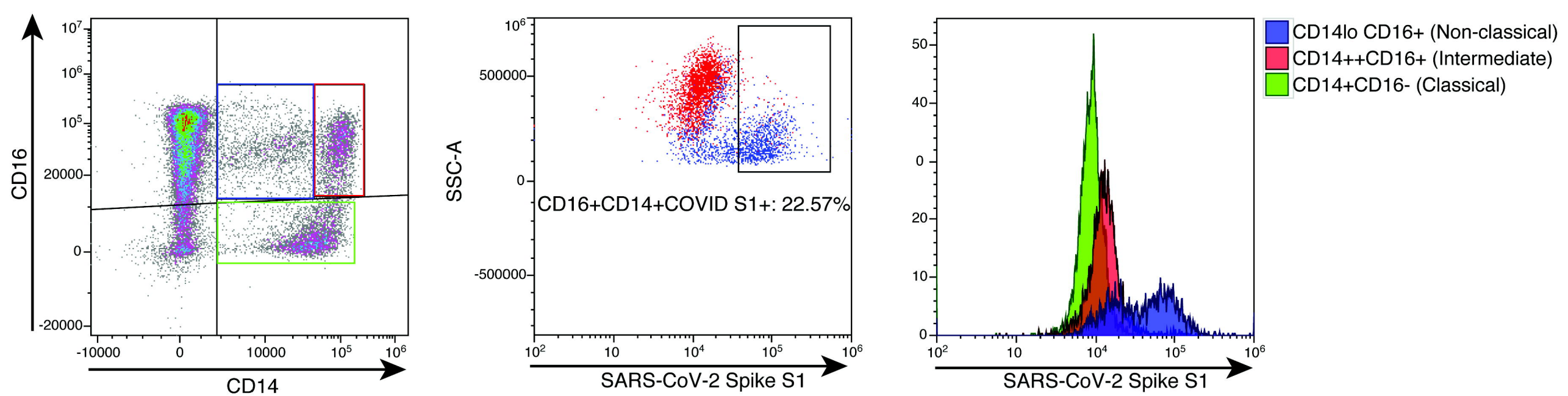
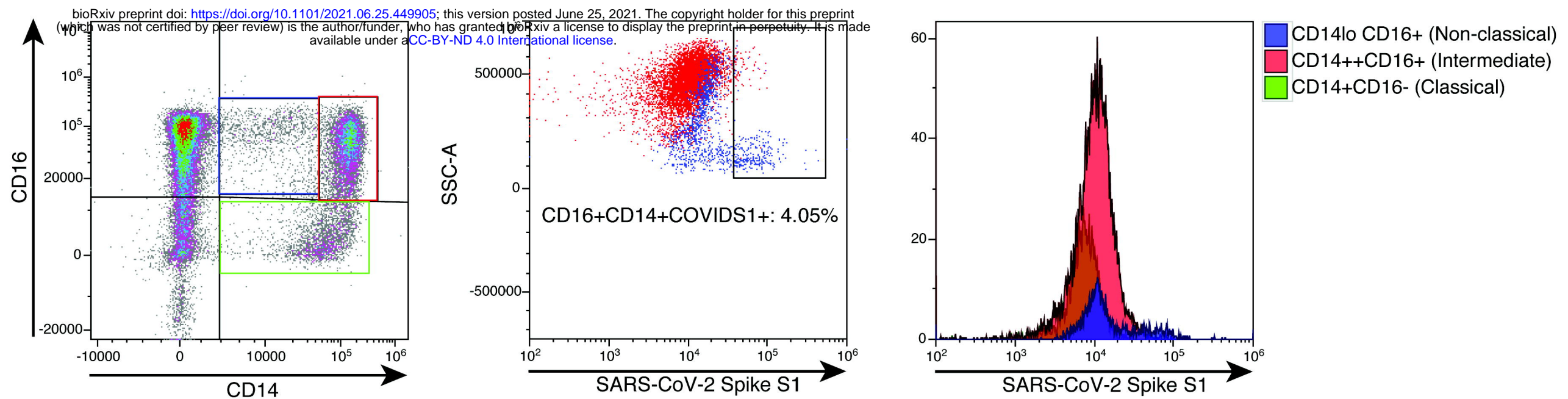
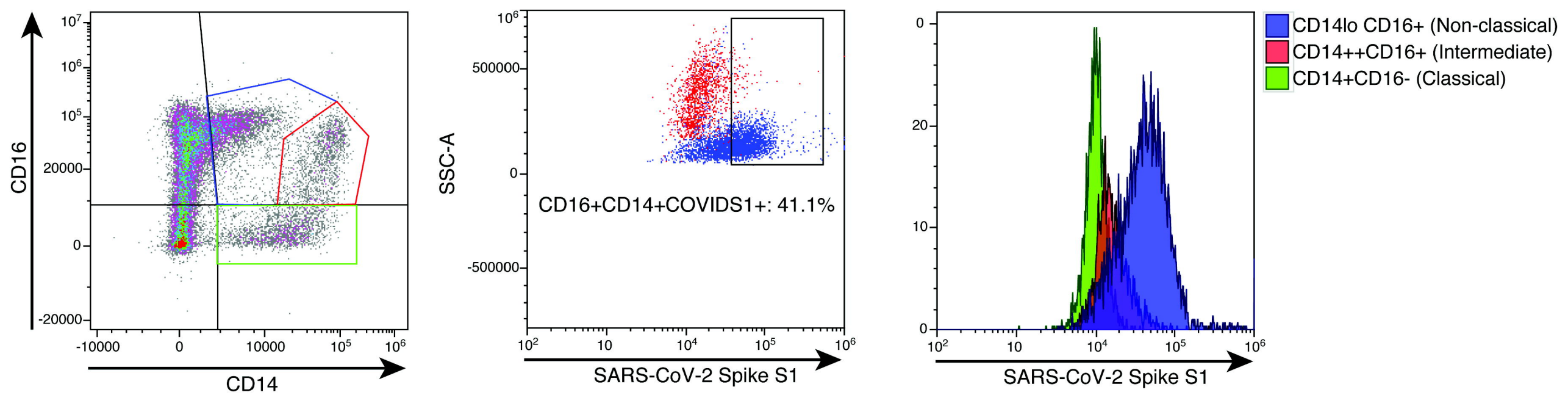
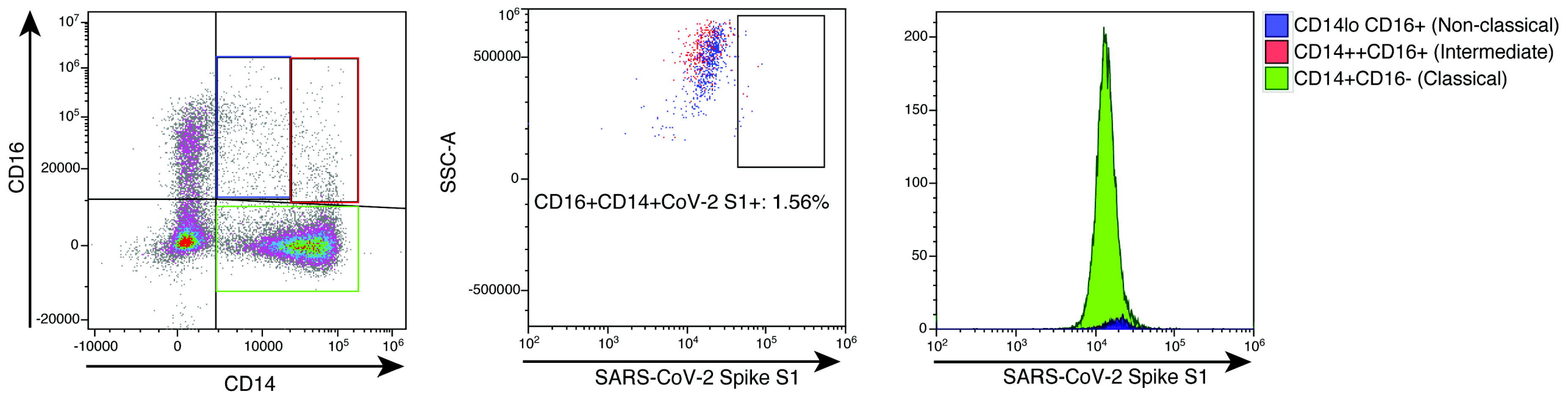
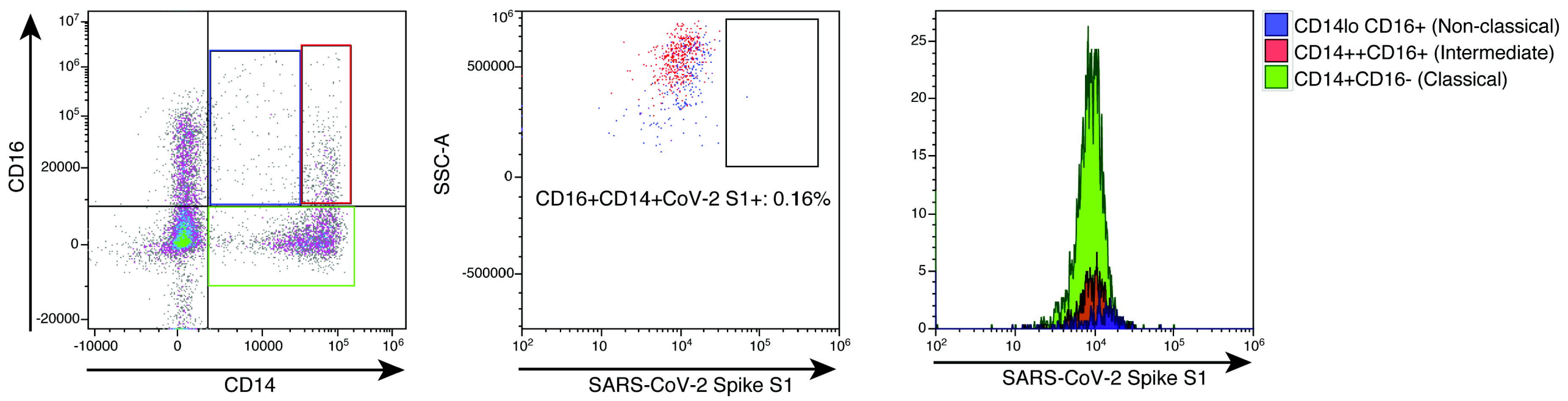
517  
518 **Figure 3.** Quantification of SARS-CoV-2 S1 protein in monocyte subsets isolated from healthy  
519 controls (HC), severe COVID-19 (severe), and PASC patients (LH). SARS-CoV-2 S1 protein  
520 was expressed in non-classical monocytes in both severe and PASC individuals. The amount of  
521 expression was statistically significant.

522  
523 **Figure 4.** LCMS confirmation of the presence of S1 subunit in samples LH1-6. A. Extracted ion  
524 chromatogram (EIC) displaying the NLREFVFK peptide. The retention time matches that of the  
525 NLREFVFK peptide in the commercial S1 standard. B. Mass Spectra of the NLREFVFK from  
526 both the commercial standard and patient LH1. The Spectra show the same mass and isotope  
527 distribution.

528



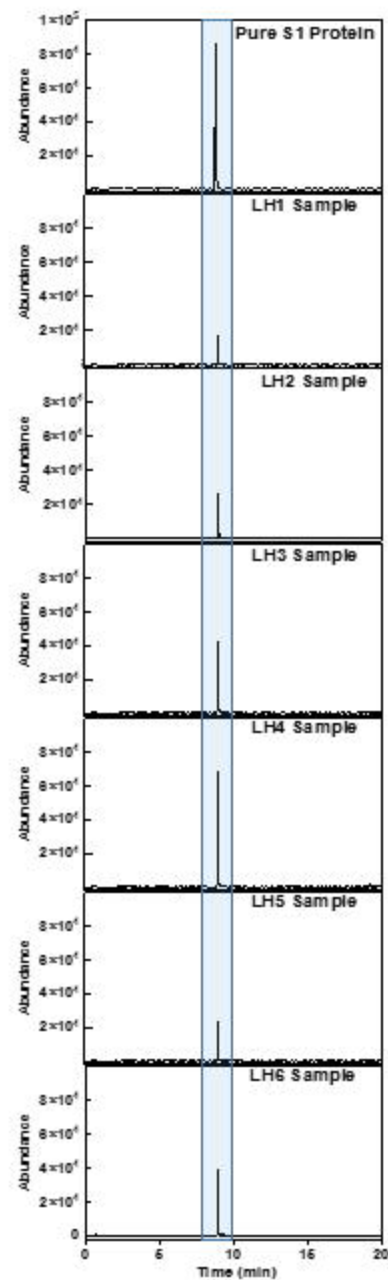




bioRxiv preprint doi: <https://doi.org/10.1101/2021.06.25.449905>; this version posted June 25, 2021. The copyright holder for this preprint (which was not certified by peer review) is the author/funder, who has granted bioRxiv a license to display the preprint in perpetuity. It is made available under aCC-BY-ND 4.0 International license.

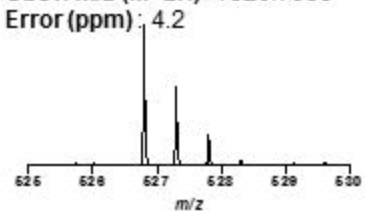


A



B

Pure S1 protein  
 Peptide sequence: NLREFVFK  
 Calc.  $m/z$  ( $M+2H$ ) $^{2+}$ : 526.7980  
 Obsv.  $m/z$  ( $M+2H$ ) $^{2+}$ : 526.7958  
 Error (ppm): 4.2



LH1 Sample  
 Peptide sequence: NLREFVFK  
 Calc.  $m/z$  ( $M+2H$ ) $^{2+}$ : 526.7980  
 Obsv.  $m/z$  ( $M+2H$ ) $^{2+}$ : 526.7954  
 Error (ppm): 4.9

